Diapycnal Mixing Induced by Rough Small-Scale Bathymetry

J. Muchowski[1,2], L. Arneborg[3], L. Umlauf[4], P. Holtermann[4], E. Eisbrenner[5], C. Humborg[1,2], M. Jakobsson[1] and C. Stranne[1,2]

[1] Department of Geological Sciences, Stockholm University, Stockholm, Sweden.

[2] Baltic Sea Center, Stockholm, Sweden.

[3] Department of Research and Development, Swedish Meteorological and Hydrological Institute, Gothenburg, Sweden.

[4] Leibniz-Institute for Baltic Sea Research, Warnemünde, Germany.

[5] Department of Meteorology, Stockholm University, Stockholm, Sweden.

Corresponding author: Julia Muchowski (julia.muchowski@geo.su.se)

Key Points:

- High-resolution turbulence observations in a shallow, strongly stratified region with extremely rough seafloor topography
- Acoustic turbulence imaging shows highly intermittent and localized mixing due to wake eddies and internal-wave breaking near obstacles
- Strongly enhanced mixing due to bathymetric features, causing hotspots of mixing in the Baltic Sea

Abstract

We investigate the effect of extremely rough bathymetry on energy dissipation and mixing in a coastal region characterized by small-scale seafloor features penetrating a strongly-stratified density interface of comparable vertical scale. Our data from the non-tidal Baltic Sea include shear microstructure measurements and observations from a broadband echosounder, here used to resolve the extreme variability and intermittency of stratified turbulence in the vicinity of obstacles. Scale analysis and acoustic imaging of small-scale turbulent motions suggest that the underlying mixing mechanisms are related to topographic wake eddies and, to a smaller extent, to breaking internal waves near the bathymetric features. Vertical diffusivities exceed those at a nearby reference station with smooth bathymetry by up to two orders of magnitude. Our study emphasizes the importance of rough small-scale (< 1 km) bathymetric features for energy dissipation and vertical turbulent transport in coastal areas shaped by e.g., glacial, tectonic, or volcanic processes.

Plain Language Summary

Mixing of water across density interfaces is important for ecosystems and the circulation between basins. However, mixing related to rough small-scale bathymetry is often not resolved in models and difficult to measure. In this study, we show high-resolution acoustic observations of intense vertical mixing across a strong density interface, that separates the saltier bottom water from the fresher surface water in the northern Baltic Sea. In the study region, steep underwater hills and ridges extend into the density interface. As water flows over the region, the hills and ridges cause the water to mix. Measured values of mixing and vertical salt fluxes in this region are up to two orders of magnitude higher than at a nearby reference station with smooth bathymetry. Our analysis suggests that the observed high mixing is mainly caused by eddies in the wake of obstacles and secondarily by breaking internal waves, which are waves within the water that occur on interfaces between layers with different properties. Understanding mixing mechanisms and estimating their contribution is needed to implement mixing into ocean models. This study highlights the importance of rough small-scale seafloor features (< 1 km) for mixing and vertical transport of heat and matter.

Keywords: diapycnal mixing, rough small-scale bathymetry, stratified flow over obstacles, broadband acoustic observations of turbulent mixing, microstructure profiler turbulence measurements, mixing across halocline

1 Introduction

Rough bathymetry is known to considerably increase vertical mixing in the deep ocean (Polzin et al. 1997; Ledwell et al. 2000; Garabato et al. 2004; Kunze et al. 2006; Nikurashin and Legg 2011; Waterhouse et al. 2014), in fjords (Arneborg & Jansson, 2017), and in lakes (Wüest & Lorke, 2003). Several mechanisms have been shown to result in enhanced mixing near rough bathymetry. Processes related to internal-wave generation (Alford et al., 2011; Garrett & Kunze, 2007; MacKinnon et al., 2017; Nycander, 2005), hydraulic effects (Alford et al., 2013; Arneborg & Jansson, 2017; Legg & Klymak, 2008), and the shedding of eddies in the wake of topographic obstacles (Caldeira et al., 2005; MacKinnon et al., 2019; Pawlak et al., 2003; Perfect et al., 2020) are believed to be particularly relevant. However, field studies of these processes, typically based on in-situ profiling measurements, were generally unable to capture the extreme spatial heterogeneity and intermittency of turbulence near bathymetric features, and focused only on individual obstacles rather than the overall effect in regions with extremely rough bathymetry.

Here, we combine traditional turbulence microstructure profiling measurements with a new type of high-resolution broadband acoustic turbulence observations to investigate the effect of extremely rough bathymetry on energy dissipation and mixing in a coastal region characterized by a large number of topographic features (hills and ridges) penetrating into a strongly stratified density interface. Our study area in the Southern Quark, northern Baltic Sea, is known for its rough small-scale bathymetry (Jakobsson et al., 2019) with horizontal scales O_h(100 m) and a large potential for enhanced mixing (Nohr & Gustafsson, 2009). While most previous studies that investigate mixing related to rough bathymetry have focused on tidal currents, we present a dataset practically not influenced by tides. Our study points at the relevance of seafloor-ocean interactions in coastal regions with strongly corrugated bathymetry which lead to enhanced energy dissipation and vertical transports of nutrients and oxygen and therefore may have an important regulatory effect on the development of oxygen minimum zones.

2 Study Area and Methods

The study area in the Southern Quark is located at the border between the Bothnian and Åland seas (Fig. 1). It constitutes a major oceanographic bottleneck in which the bathymetry controls water exchange between two of the Baltic Sea's main basins (Elken & Matthäus, 2008). The particularly rough seafloor is due to the underlying bedrock geology, tectonic lineaments (Beckholmen & Tiren, 2009), and interaction between the seafloor and the Scandinavian Ice Sheet (Greenwood et al., 2017). Here we use the gridded bathymetric model compiled by EMODnet at a grid-cell resolution of 1/16 arc minute (EMODnet Bathymetry Consortium, in prep) to assess the seafloor morphology. The version we use is scheduled to be published before the end of 2022 and includes multibeam bathymetry in the Southern Quark acquired with Stockholm University's Research Vessel R/V *Electra* in 2017 (Jakobsson et al., 2019).

Oceanographic and acoustic data presented in this study were collected during a cruise with R/V *Electra* on 2-3 March 2020 on six transects in a region of particularly rough bathymetry and a reference station located in a deeper and topographically smooth basin bounding the study area in the east and south (Fig. 1). Oceanographic data were collected with a free-falling MSS-90L microstructure profiler (MSS) from Sea&Sun Technology (SST, Germany), equipped with two PNS06 airfoil shear probes for estimates of the dissipation rate of turbulent kinetic energy, a FP07 fast-response thermistor, precision CTD (Conductivity, Temperature, Depth) sensors, and an oxygen sensor. All sensors were sampled at 1024 Hz and digitized at 16-bit resolution. The sinking velocity of the profiler was adjusted to about 0.7 m s^{-1}. In total, 50 MSS casts were collected, of which 47 casts are located in the study region and three casts at the reference station (Fig. 1 a and c). From the MSS profiles, conservative temperature Θ, absolute salinity S_A, and buoyancy frequency N were computed according to the international TEOS-10 standard for seawater (IOC et al. 2010). Detailed information on the processing of MSS shear microstructure data is found in (Muchowski et al., 2022). The location of the transects and positioning of the MSS casts was based on real-time acoustic observations as described in the next section.

Acoustic observations were conducted with a Simrad ES70-7C (45-90 kHz) split beam transducer (Kongsberg, Norway) in combination with a Simrad EK80 wideband transceiver, using a ping rate of 1 Hz and a pulse duration of 4.1 ms. The received signal was processed using pulse compression and compensated for spherical spreading and absorption. The system was calibrated in the study area during the measuring campaign with a 38.1-mm tungsten carbide

sphere, as described in Demer et al. (2015). R/V *Electra's* Seapath 330+ RTK GPS unit and a MRU5+ motion sensor were used for accurate positioning and compensation of (wave-induced) heave in the acoustic observations. We show calibrated acoustic backscatter strength per volume (S_v) in dB re 1µPa.

While the MSS profiler measures small-scale turbulent velocity fluctuations, the EK80 measures acoustic backscatter from density and sound speed fluctuations, caused by temperature and salinity fluctuations (e.g. Lavery et al. 2013). Therefore, acoustics only register turbulent structures in regions with existing background temperature and salinity gradients, where turbulent stirring induces temperature and salinity microstructure and thus increased acoustic backscatter (Muchowski et al., 2022), whereas MSS measurements show dissipation rates also in well-mixed parts of the water column. Thus, the acoustic observations indicate regions where mixing of different water masses occurs and where the diapycnal transport of salt and/or heat is increased. Additionally, the EK80 records strong backscatter from biological scatterers, such as zooplankton and fish, in this dataset. Muchowski et al. (2022) showed that in areas where biological scattering does not dominate the signal, turbulent microstructure is the primary source of acoustic backscatter recorded with the R/V *Electra* EK80 system in this region and time of year. In this study, we conducted acoustic surveys to identify regions of increased stratified mixing prior to our MSS measurements. These real-time acoustic observations enabled us to plan positions of the MSS measurements and to target local mixing hotspots in a region with complex and highly intermittent turbulence.

Acoustic Doppler Current Profiler (ADCP) data were collected using *Electra's* hull-mounted 600 kHz Workhorse ADCP (Teledyne RDI, USA) (see Supplementary Fig. S1). This instrument provided reliable data down to 40-50 m water depth and therefore did not include most of the halocline region below approximately 50 m depth.

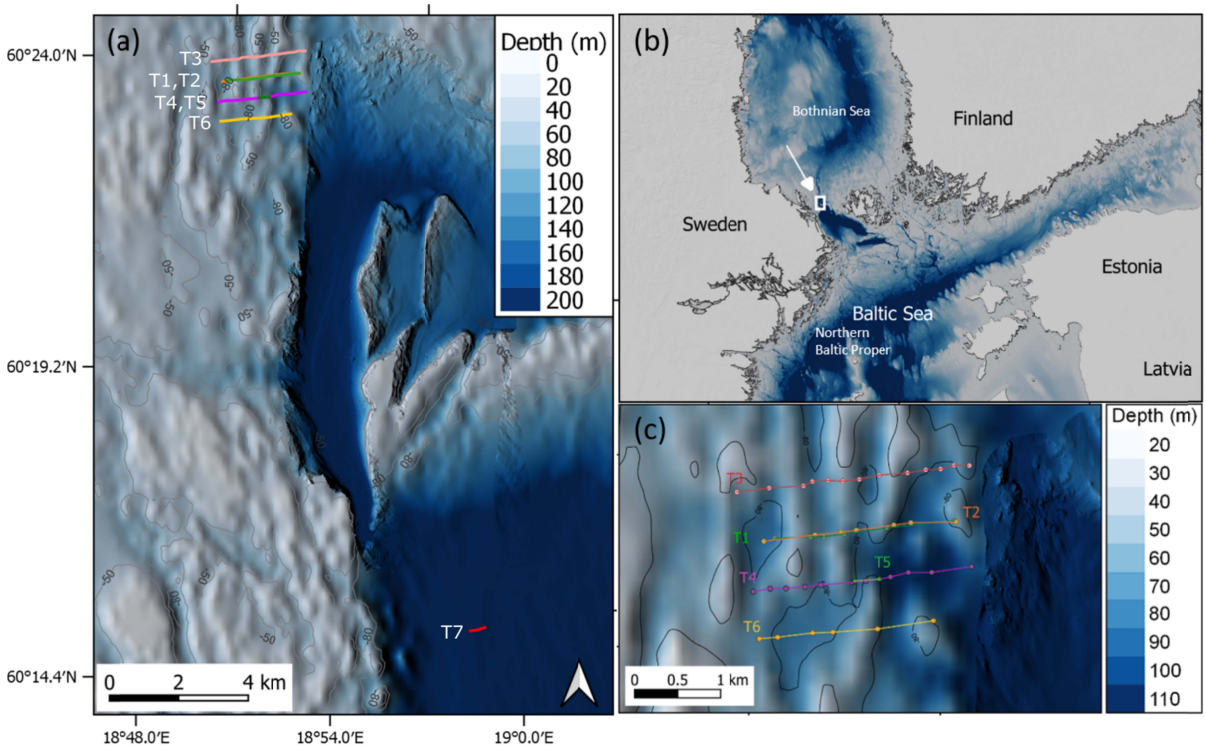

Figure 1: Bathymetry of the study area in the Åland Sea: (a) Overview map with MSS transects T1-T7 marked by colored lines (MSS casts 76-125, collected between 2 March 2020, 14:45 UTC and 3 March 2020, 17:10 UTC). (b) overview map of northern Baltic Sea with study region in the Åland Sea shown in (a) marked by white rectangle; (c) main study region with transects T1-T6 enlarged. Each dot represents a MSS cast. Background bathymetry data from EMODnet (EMODnet Bathymetry Consortium 2020), detailed multibeam bathymetry data in (a) and (c) acquired by R/V Electra and granted public release by the Swedish Maritime Administration (release 17-03187).

To estimate turbulent mixing, the turbulent vertical diffusion coefficient k_z is calculated from the dissipation rate of turbulent kinetic energy ε, following the Osborn (1980) model:

$$k_z = \gamma\, \varepsilon\, N^{-2}, \tag{1}$$

where N is the buoyancy frequency of the background stratification and γ the flux coefficient, here assumed to be equal to 0.2 (Gregg et al., 2018).

The vertical transport due to turbulent mixing, F_{zX}, of a tracer, X (e.g. salinity, heat, oxygen, nutrients) is calculated from Fick's law

$$F_{zX} = -k_z \cdot \frac{\partial X}{\partial z} \cdot \rho\ , \tag{2}$$

where z is defined positive upward and ρ is the water density.

3 Results and Discussion

3.1 In-situ measurements

Microstructure (MSS) profiles of conservative temperature Θ, absolute salinity S_A, and buoyancy frequency N show that the stratification in the study area (transect T1-T7, Fig. 1c) is characterized by a halocline between 50-80 m water depth, which separates warmer and saltier deep water from a cooler and fresher surface layer (Fig. 2). The entire water column is stably stratified with a buoyancy frequency that ranges from $N^2 = 10^{-6}$ s^{-2} in the surface- and bottom layers to $N^2 = 10^{-3}$ s^{-2} in the halocline.

To isolate the effect of the corrugated topography in the study area, we compare our data to reference transect T7, south of the study region (Fig. 1a, in red), where we expect a similar meteorological forcing but no significant topographic effects due to the larger water depth and the smooth seafloor. At this reference station, the halocline is shallower and broader but shows comparable maximum values for N^2 (Fig. 2). The vertical offset in halocline depth implies a baroclinic pressure gradient favoring a northward transport of deep water. This transport, and the mixing processes studied in the following, are important components of the estuarine circulation of the Northern Baltic Sea, determining water mass properties and ventilation of the deep water.

MSS profiles of kinetic energy dissipation rates, ε, vertical turbulent diffusivity, k_z, and vertical salt flux, F_{zS}, show that all three quantities are increased by up to two orders of magnitude in the halocline of the study region (Fig. 2d-f). The average dissipation rate in the halocline of all 47 MSS profiles in the study region is $\approx 1.1 \cdot 10^{-7}$ W kg^{-1} and thereby two orders of magnitude above measurements at the reference station. Average vertical diffusivities are $\approx 7 \cdot 10^{-4}$ m^2 s^{-1} in the halocline of the study area, while average vertical diffusivities at the reference station as well as in other parts of the Baltic Sea are measured to be 1-2 orders of magnitude lower. For example, $k_z < 10^{-5}$ m^2 s^{-1} in the halocline of the Eastern Gotland Basin (Lass, 2003). The mean salinity flux through the halocline (50-80 m depth), calculated from (2) and averaged over all MSS profiles in the study region is $F_{zS} = 0.01$ kg m^{-2} s^{-1}. While salinities in the study area are overall lower than in the Baltic Proper, the diapycnal salinity flux is one order of magnitude above the average in

the entire Baltic Sea, including upwelling (Reissmann et al. 2009), as well as in the Bornholm (van der Lee & Umlauf, 2011) and Eastern Gotland Basin (Rahm 1985).

To investigate the impact of the observed mixing rates on the evolution of the halocline and the adjacent surface and deep-water layers, we numerically solved the one-dimensional diffusion equation with a vertically variable diffusivity, approximated as $k = \min(\alpha N^{-1}, k_{max})$ (Stigebrandt 1987, equation 2.2), with $\alpha = 5 \cdot 10^{-6}$ and $k_{max} = 10^{-2}$ m^2 s^{-1}. With these parameters, the model reproduces the observed diffusivities in the halocline, and has the advantage, compared to a model with a prescribed (fixed) diffusivity profile, that the diffusivity dynamically adapts to the evolution of the halocline. The initial conditions are chosen to approximate the observed salinity profile by an inverse tangent function. Model results show (Fig. 3) that the halocline width nearly doubles and that salinities in the layers above and below the halocline are modified by about 0.1 g kg^{-1} over a period of 5 days, which would correspond to a typical residence time for surface-layer waters in the study area (horizontal scale: 20 km) for typical current speeds of 0.05 m s^{-1} (see supplementary Fig. S1). As the larger-scale forcing of deep-water flow in the area is predominantly northward, the modification of the water below the halocline due to the observed mixing may be relevant for the deep-water conditions in the Bothnian Sea, adjacent to the north of the study region.

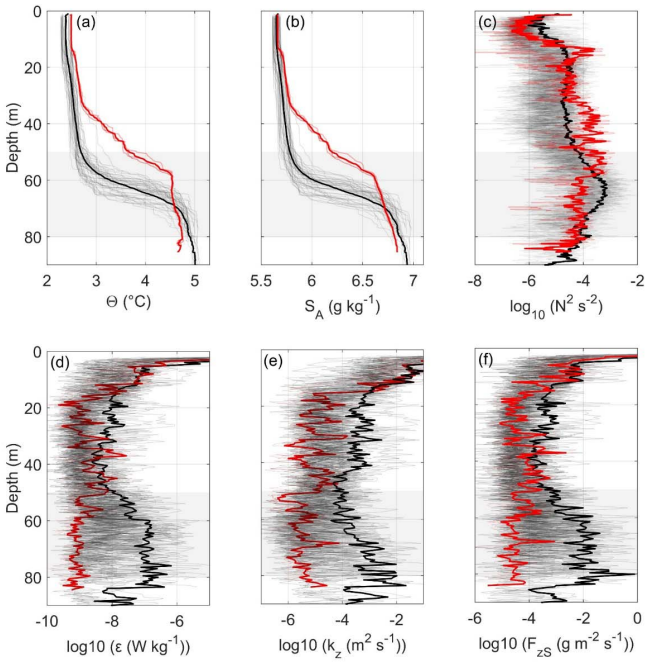

Figure 2: (a) Conservative temperature (Θ), (b) absolute salinity (S_A), (c) buoyancy frequency (N^2), (d) dissipation rate of turbulent kinetic energy (ε), (e) vertical turbulent diffusivity (k_z) and vertical salt flux (F_{zS}) from 47 MSS casts in the study region (black) and 3 MSS casts at the reference station (red) together with their arithmetic mean values (bold). Positions of MSS casts are shown on map in Fig. 1 (MSS 76-125). Grey shaded patch marks the halocline in the study region.

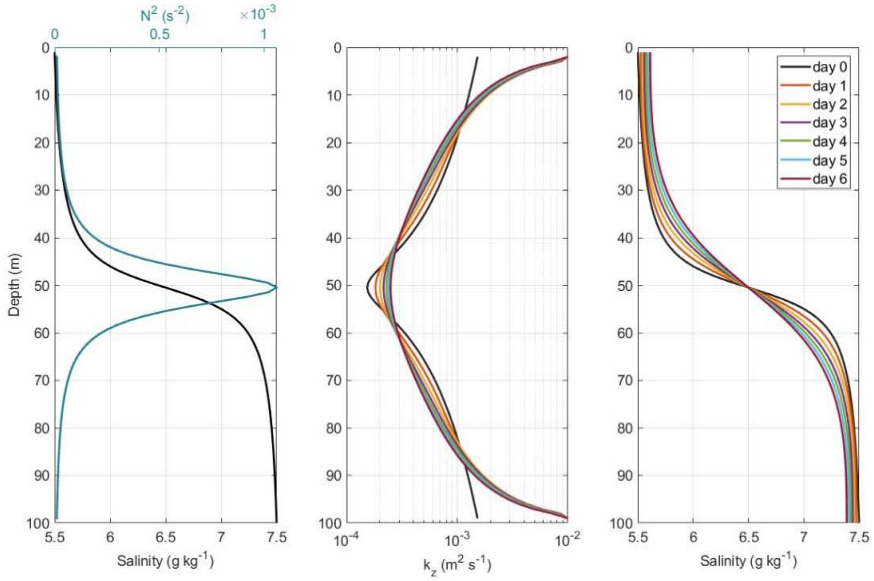

Figure 3: Diffusion model of the study region. (a) initial salinity profile and corresponding buoyancy frequency, (b) initial turbulent vertical diffusivity profile (blue) and its development over time, (c) initial salinity profile (blue) and its development over time.

3.2 Broadband acoustic observations

The unique advantage of acoustic observations compared to the traditional microstructure profiling described above lies in their extreme spatial resolution, revealing the complex geometry and intermittency of mixing near topographic obstacles in a level of detail usually available only from turbulence-resolving numerical simulations (Puthan et al., 2022). Figure 4 shows that mixing in our study area occurs in confined regions, especially near hilltops that reach into the halocline and in detached mixing bands that are horizontally correlated on scales of 0.1 – 1 km. Overall, we see an excellent one-to-one correspondence between regions with enhanced acoustic backscatter and enhanced energy dissipation from shear microstructure (Fig. 4a), and in some cases also good quantitative agreements in the inferred dissipation rates (Fig. 4c) in all six transects (not shown here).

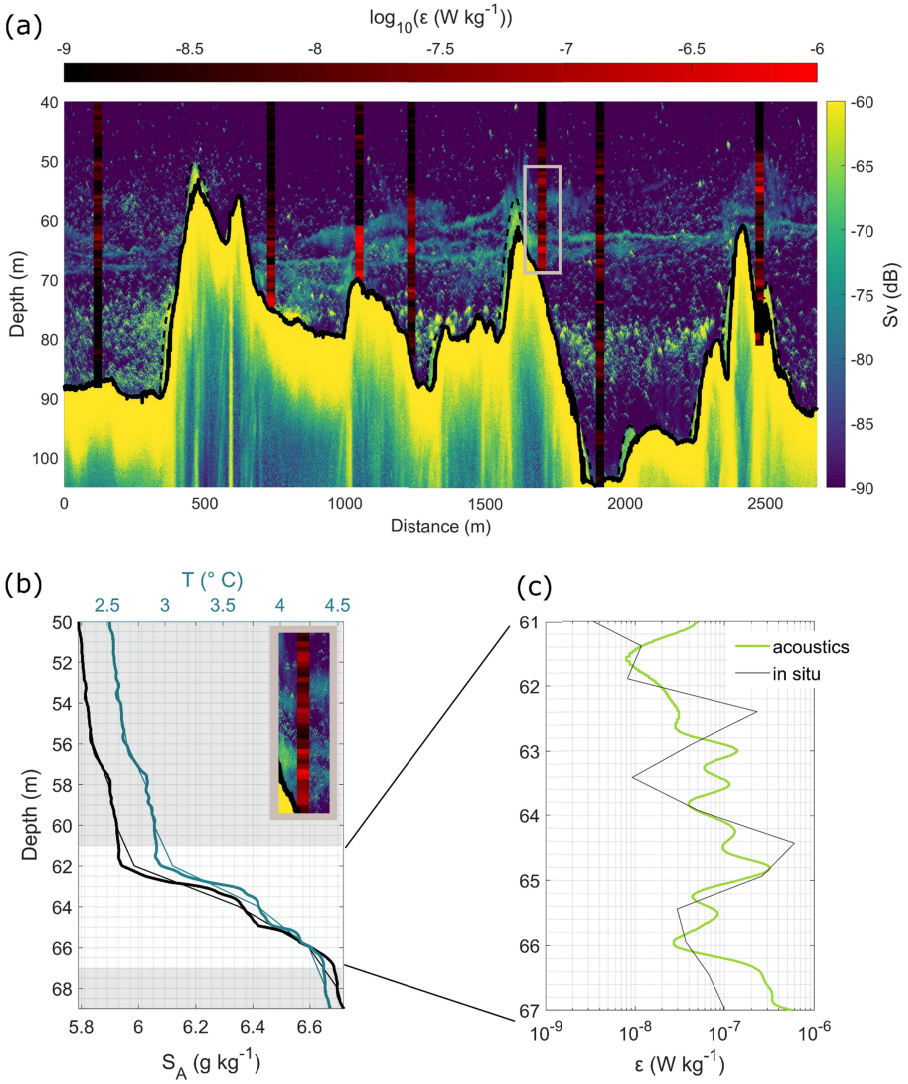

Figure 4: (a) EK80 echogram showing transect T2, sampled 3 March 2020, 09:08-10:00 UTC, with seafloor bathymetry marked in black, sidelobes marked by dashed black line. Vertical profiles show dissipation rates from MSS casts 82-88, color-coded in red.

(b) conservative temperature (turquoise) and absolute salinity (black) profile from MSS 86, (c) dissipation rate ε from MSS cast 86 (black) and inferred from acoustic backscatter (green) in combination with temperature and salinity profile shown in (b).

Quantitative estimates of energy dissipation rates from acoustic observations in between microstructure profiles are complicated by the lack of commensurate observations of temperature and salinity stratification (extrapolations are highly inaccurate due to the strong spatial variability in this region). Additionally, the acoustic signal is often dominated by biological scattering, especially in the deeper layers below 70 m. We therefore avoid quantitative estimates and integration of dissipation rates based on acoustic backscatter. Nevertheless, the acoustic measurements provide a tool to visualize and map turbulent mixing at high resolution which would not be achievable with any of the traditional techniques to observe turbulence.

3.3 Mixing mechanisms

Local mixing hotspots seen in Figure 4 are likely caused by a combination of mixing mechanisms related to the rough bathymetric features. To analyze the relevance of different potential mixing mechanisms, we define the most important bulk parameters characterizing the study area: h = 20 m as a typical vertical scale of the bathymetric features (as seen in Fig. 4a), L_N = 30 m as the thickness of the halocline (Fig. 2b), N = 0.015 s^{-1} for the average buoyancy frequency in the halocline (Fig. 2c), $f = 1.26 \cdot 10^{-4}$ s^{-1} for the Coriolis parameter, and u = 0.05 m s^{-1} for typical velocities at the bottom of the ADCP range, i.e. at the upper end of the halocline region (see Supplementary Fig. S1). The latter estimate is the most uncertain as the currents are fluctuating and measurements in the core of the halocline are lacking. Finally, the lateral scales of bathymetric features in this study are anisotropic, ranging from values of the order d = 500 m in the cross-ridge (west-east) direction to d = 2000 m in the along-ridge (north-south) direction, respectively (Fig. 1c).

Based on the above defined parameters, the non-dimensional topographic Froude number $Fr = u/(Nh)$ can be estimated to ≈ 0.17. The small Froude number suggests that much of the flow is blocked or, where possible, flows around the bathymetric features. Near the hilltops, however, overflow could be possible. The Rossby number is $Ro = u/(fd) \approx 0.2 - 0.8$, where the smaller and larger values of Ro correspond to our along-ridge and cross-ridge estimates of d. These small to moderate values suggest that the flow is significantly affected by rotation. The intrinsic frequency of lee waves, $\omega = 2\pi u/d$, is about $(1.6 - 6.3) \cdot 10^{-4}$ s^{-1} which is larger than f

but much smaller than *N*, meaning that lee waves are possible but propagate with nearly horizontal phase lines. Possible mixing mechanisms are therefore to some extent breaking internal lee waves due to flow over bathymetric features, but more importantly, lee vortices or wake eddies due to flow around them and nonlinear hydraulic effects due to topographic blocking. Our observations show similarities to model studies of wake eddies from Puthan et al. (2020 and 2022), carried out at a topographic Froude number of 0.2 and 0.15, respectively but for a single hill and at a much larger Rossby number where rotation is less important. Puthan et al. (2022) pointed out that consistently higher dissipation rates are observed inside the thin hydraulic jet evolving at the apex of an obstacle for low *Fr* (see their figure 7). The thin, banded structures of enhanced backscatter visible in both our EK80 and shear-microstructure measurements near the top of obstacles (Fig. 4) could be interpreted as evidence for this process (unfortunately, our ship ADCP data do not reach down to this region).

These qualitative arguments can be substantiated with the help of shear microstructure measurements and theoretical energy dissipation estimates. Energy dissipation due to topographic wake eddies is suggested to scale as u^3/d (e.g., Puthan et al. 2022), yielding dissipation rates in the range [0.6 - 2.5] $\cdot 10^{-7}$ W kg^{-1}, i.e. of the same order of magnitude as our observations ($\approx 1.1 \cdot 10^{-7}$ W kg^{-1}). The integrated dissipation rate (based on the average dissipation rate $\bar{\varepsilon}$ of all 47 MSS profiles) in the halocline of the study region is

$$D_i = \int_{z=50\,\mathrm{m}}^{z=80\,\mathrm{m}} \bar{\varepsilon}\,\rho\,\mathrm{d}z \approx 3.4\mathrm{mW\,m^{-2}}\,. \qquad (3)$$

Assuming that the dissipation rate scaling u^3/d is relevant for the halocline, the depth integrated dissipation, corresponding to (3), would scale as $\rho u^3 L_N/d$, where L_N is the thickness of the halocline. With the parameters defined above, the resulting integrated dissipation rates are in the range [1.3-5.2] mW m^{-2}, close to the observed value. Note that this parametrization for wake eddies is independent of stratification.

Integrated energy dissipation due to internal wave generation at topography in the ocean and the atmosphere is suggested to scale as $\rho N u^2 h^2/d$ in the linear limit, e.g. (Arneborg & Jansson, 2017; St. Laurent et al., 2002; Stigebrandt, 1976; Welch et al., 2001) and includes stratification. Using this scaling results in values of D_i in the range [8-31] mW m^{-2}, i.e. larger than the

observed value (3). Previous studies of tidal stratified flow over steep topography (Arneborg & Jansson, 2017; St. Laurent et al., 2002) have shown that about 20% to 30% of the energy flux calculated with this scaling is dissipated locally. This leads to estimates of D_i in the right order of magnitude as (3), with more comparable values for horizontal scales of 2000 m. Studies of atmospheric lee-waves also show a strong decrease in integrated energy conversion to lee waves relative to the linear limit for small Froude numbers (e.g. Welch et al. 2001) which means that the observed value can be in agreement with those results. There are, however, no clear signs of oblique bands that would be expected from breaking internal lee waves. This suggests either that these are not present or that they are horizontal due to the perpendicular transect relative to the northward flow.

4 Conclusions

We present in-situ microstructure measurements of dynamic turbulent diapycnal mixing near steep small-scale bathymetric hills and ridges that reach into stratified flow. Collocated acoustic observations of stratified mixing are consistent with shear-microstructure measurements but have much higher vertical and horizontal resolution. Thus, providing insights into the complex anatomy of the mixing, including hotspots of mixing near the summits and crests of the particularly rough bathymetric features. The acoustic observations thereby enable us to map turbulent mixing at unprecedented resolution and to plan in-situ measurements accordingly. We suggest that the observed mixing mechanisms, which here increase dissipation rates by one to two orders of magnitude, could play an important role beyond our study region, such as in large parts of the Bothnian Sea as well as coastal areas in the Baltic Sea and around the globe where rough, small-scale bathymetry reaches into stratified flow.

Energy conversion and turbulence scalings for both, topographic wake eddies and internal waves, are to some degree supported by our integrated measured dissipation rates. However, the acoustically observed thin, horizontal, laterally coherent bands of high dissipation are similar to what has been shown for idealized stratified flow around seamounts. Additionally, the estimated Froude number of 0.17 points towards the process of wake eddy generation from flow around obstacles more than that of breaking lee waves from flow over obstacles. This could have large impacts on parametrizations, as the scaling of energy dissipation due to wake eddies is

fundamentally different from that of internal wave generation, which has usually been assumed to cause mixing above rough seafloor topography. Besides the potential to improve parameterizations of this kind of mixing in models which do not resolve the flow above such bathymetry, a better understanding of the underlying mechanisms may even lead to improved drag parameterizations and thereby more accurate currents and transports in the models, as has been shown to be the case for atmospheric models (Alexander et al., 2010).

The combination of a bathymetry roughness index based on high-resolution multibeam data with suitable mixing parameterizations based on stratification and current velocities could potentially improve the ocean component of global, regional, and coastal climate models significantly.

More observational data as well as model studies of stratified flow over small-scale bathymetry are needed to fully capture the extent of the described processes, discriminate between them and gauge their importance. Future studies could involve a portable autonomous broadband echosounders, either towed, mounted on a CTD rosette, or mounted on gliders for measurements at greater depths.

Acknowledgments

We thank Martin Sass (IOW, Warnemunde, Germany) for technical support with MSS profilers during the cruise. We thank Florian Roth, Ole Pinner and Emelie Ståhl for participating in data collection. We thank the captain Thomas Strömsnäs and the crew Mattias Murphy, Carl-Magnus Wiltén and Albin Knochenhauer of R/V Electra for their assistance and support.

Open Research

Data will be published and made accessible for downloading on the Bolin Centre Database website (https://bolin.su.se/data) prior to publication. Data are already now available on the Bolin Centre Database in the unpublished project:
https://bolin.su.se/data/contributions/?d=8761&p=MjAyMi0xMi0xNiAwOTo1Njo1Ny42MzcxMTYgNDQ4MDMyMTE

References

345 Alexander, M. J., Geller, M., McLandress, C., Polavarapu, S., Preusse, P., Sassi, F., Sato, K., Eckermann, S., Ern,
346 M., & Hertzog, A. (2010). Recent developments in gravity-wave effects in climate models and the global
347 distribution of gravity-wave momentum flux from observations and models. *Quarterly Journal of the Royal*
348 *Meteorological Society*, *136*(650), 1103–1124.
349 Alford, M. H., Girton, J. B., Voet, G., Carter, G. S., Mickett, J. B., & Klymak, J. M. (2013). Turbulent mixing and
350 hydraulic control of abyssal water in the Samoan Passage. *Geophysical Research Letters*, *40*(17), 4668–
351 4674. https://doi.org/10.1002/grl.50684
352 Alford, M. H., MacKinnon, J. A., Nash, J. D., Simmons, H., Pickering, A., Klymak, J. M., Pinkel, R., Sun, O.,
353 Rainville, L., Musgrave, R., Beitzel, T., Fu, K.-H., & Lu, C.-W. (2011). Energy Flux and Dissipation in
354 Luzon Strait: Two Tales of Two Ridges. *Journal of Physical Oceanography*, *41*(11), 2211–2222.
355 https://doi.org/10.1175/JPO-D-11-073.1
356 Arneborg, L., & Jansson, R. (2017). Tidal Energy Loss, Internal Tide Radiation, and Local Dissipation for Two-
357 Layer Tidal Flow over a Sill. *JOURNAL OF PHYSICAL OCEANOGRAPHY*, *47*, 18.
358 Beckholmen, M., & Tiren, S. A. (2009). *The geological history of the Baltic Sea. A review of the literature and*
359 *investigation tools*. https://www.osti.gov/etdeweb/biblio/963502
360 Caldeira, R. M. A., Marchesiello, P., Nezlin, N. P., DiGiacomo, P. M., & McWilliams, J. C. (2005). Island wakes in
361 the Southern California Bight. *Journal of Geophysical Research: Oceans*, *110*(C11).
362 https://doi.org/10.1029/2004JC002675
363 Demer, D. A., Berger, L., Bernasconi, M., Bethke, E., Boswell, K., Chu, D., Domokos, R., Dunford, A., Fassler, S.,
364 Gauthier, S., Hufnagle, L. T., Jech, J. M., Bouffant, N., Lebourges-Dhaussy, A., Lurton, X., Macaulay, G.
365 J., Perrot, Y., Ryan, T., Parker-Stetter, S., … Williamson, N. (2015). *Calibration of acoustic instruments.*
366 [Report]. International Council for the Exploration of the Sea (ICES). https://doi.org/10.25607/OBP-185
367 Elken, J., & Matthäus, W. (2008). Assessment of Climate Change for the Baltic Sea Basin. *Baltic Sea*
368 *Oceanography*, 379–385.
369 EMODnet Bathymetry Consortium (2020): EMODnet Digital Bathymetry (DTM).
370 https://doi.org/10.12770/bb6a87dd-e579-4036-abe1-e649cea9881a

Garabato, A. C. N., Polzin, K. L., King, B. A., Heywood, K. J., & Visbeck, M. (2004). Widespread Intense Turbulent Mixing in the Southern Ocean. *Science*, *303*(5655), 210–213. https://doi.org/10.1126/science.1090929

Garrett, C., & Kunze, E. (2007). Internal tide generation in the deep ocean. *Annu. Rev. Fluid Mech.*, *39*, 57–87.

Greenwood, S. L., Clason, C. C., Nyberg, J., Jakobsson, M., & Holmlund, P. (2017). The Bothnian Sea ice stream: Early Holocene retreat dynamics of the south-central Fennoscandian Ice Sheet. *Boreas*, *46*(2), 346–362. https://doi.org/10.1111/bor.12217

Gregg, M. C., D'Asaro, E. A., Riley, J. J., & Kunze, E. (2018). Mixing Efficiency in the Ocean. *Annual Review of Marine Science*, *10*(1), 443–473. https://doi.org/10.1146/annurev-marine-121916-063643

IOC, SCOR and IAPSO, 2010: The international thermodynamic equation of seawater - 2010: Calculation and use of thermodynamic properties. Intergovernmental Oceanographic Commission, Manuals and Guides No. 56, UNESCO (English), 196 pp.

Jakobsson, M., Stranne, C., O'Regan, M., Greenwood, S. L., Gustafsson, B., Humborg, C., & Weidner, E. (2019). Bathymetric properties of the Baltic Sea. *Ocean Science*, *15*(4), 905–924. https://doi.org/10.5194/os-15-905-2019

Kunze, E., Firing, E., Hummon, J. M., Chereskin, T. K., & Thurnherr, A. M. (2006). Global Abyssal Mixing Inferred from Lowered ADCP Shear and CTD Strain Profiles. *Journal of Physical Oceanography*, *36*(8), 1553–1576. https://doi.org/10.1175/JPO2926.1

Lass, H. U. (2003). Dissipation in the Baltic proper during winter stratification. *Journal of Geophysical Research*, *108*(C6), 3187. https://doi.org/10.1029/2002JC001401

Lavery, A. C., Geyer, W. R., & Scully, M. E. (2013). Broadband acoustic quantification of stratified turbulence. *The Journal of the Acoustical Society of America*, *134*(1), 40–54. https://doi.org/10.1121/1.4807780

Ledwell, J. R., Montgomery, E. T., Polzin, K. L., St. Laurent, L. C., Schmitt, R. W., & Toole, J. M. (2000). Evidence for enhanced mixing over rough topography in the abyssal ocean. *Nature*, *403*(6766), 179–182. https://doi.org/10.1038/35003164

Legg, S., & Klymak, J. (2008). Internal Hydraulic Jumps and Overturning Generated by Tidal Flow over a Tall Steep Ridge. *Journal of Physical Oceanography*, *38*(9), 1949–1964. https://doi.org/10.1175/2008JPO3777.1

399 MacKinnon, J. A., Alford, M. H., Voet, G., Zeiden, K. L., Shaun Johnston, T. M., Siegelman, M., Merrifield, S., &
400 Merrifield, M. (2019). Eddy Wake Generation From Broadband Currents Near Palau. *Journal of*
401 *Geophysical Research: Oceans*, *124*(7), 4891–4903. https://doi.org/10.1029/2019JC014945
402 MacKinnon, J. A., Zhao, Z., Whalen, C. B., Waterhouse, A. F., Trossman, D. S., Sun, O. M., Laurent, L. C. S.,
403 Simmons, H. L., Polzin, K., Pinkel, R., Pickering, A., Norton, N. J., Nash, J. D., Musgrave, R., Merchant,
404 L. M., Melet, A. V., Mater, B., Legg, S., Large, W. G., … Alford, M. H. (2017). Climate Process Team on
405 Internal Wave–Driven Ocean Mixing. *Bulletin of the American Meteorological Society*, *98*(11), 2429–
406 2454. https://doi.org/10.1175/BAMS-D-16-0030.1
407 Muchowski, J., Umlauf, L., Arneborg, L., Holtermann, P., Weidner, E., Humborg, C., & Stranne, C. (2022).
408 Potential and Limitations of a Commercial Broadband Echosounder for Remote Observations of Turbulent
409 Mixing. *Journal of Atmospheric and Oceanic Technology*.
410 Nikurashin, M., & Legg, S. (2011). A Mechanism for Local Dissipation of Internal Tides Generated at Rough
411 Topography. *Journal of Physical Oceanography*, *41*(2), 378–395. https://doi.org/10.1175/2010JPO4522.1
412 Nohr, C., & Gustafsson, B. G. (2009). Computation of energy for diapycnal mixing in the Baltic Sea due to internal
413 wave drag acting on wind-driven barotropic currents. *OCEANOLOGIA*, *51*(4), 461–494.
414 https://doi.org/10.5697/oc.51-4.461
415 Nycander, J. (2005). Generation of internal waves in the deep ocean by tides. *Journal of Geophysical Research:*
416 *Oceans*, *110*(C10). https://doi.org/10.1029/2004JC002487
417 Pawlak, G., MacCready, P., Edwards, K. A., & McCabe, R. (2003). Observations on the evolution of tidal vorticity
418 at a stratified deep water headland. *Geophysical Research Letters*, *30*(24).
419 https://doi.org/10.1029/2003GL018092
420 Perfect, B., Kumar, N., & Riley, J. J. (2020). Energetics of Seamount Wakes. Part I: Energy Exchange. *Journal of*
421 *Physical Oceanography*, *50*(5), 1365–1382. https://doi.org/10.1175/JPO-D-19-0105.1
422 Polzin, K. L., Toole, J. M., Ledwell, J. R., & Schmitt, R. W. (1997). Spatial variability of turbulent mixing in the
423 abyssal ocean. *Science*, *276*, 93–96.
424 Puthan, P., Jalali, M., Ortiz-Tarin, J. L., Chongsiripinyo, K., Pawlak, G., & Sarkar, S. (2020). The wake of a three-
425 dimensional underwater obstacle: Effect of bottom boundary conditions. *Ocean Modelling*, *149*, 101611.
426 https://doi.org/10.1016/j.ocemod.2020.101611

Puthan, P., Pawlak, G., & Sarkar, S. (2022). Wake Vortices and Dissipation in a Tidally Modulated Flow Past a Three-Dimensional Topography. *Journal of Geophysical Research: Oceans*, *127*(8), e2022JC018470. https://doi.org/10.1029/2022JC018470

Rahm, L. (1985). On the diffusive salt flux of the Baltic proper. *Tellus A*, *37A*(1), 87–96. https://doi.org/10.1111/j.1600-0870.1985.tb00272.x

Reissmann, J. H., Burchard, H., Feistel, R., Hagen, E., Lass, H. U., Mohrholz, V., Nausch, G., Umlauf, L., & Wieczorek, G. (2009). Vertical mixing in the Baltic Sea and consequences for eutrophication – A review. *Progress in Oceanography*, *82*(1), 47–80. https://doi.org/10.1016/j.pocean.2007.10.004

St. Laurent, L. C., Simmons, H. L., & Jayne, S. R. (2002). Estimating tidally driven mixing in the deep ocean: ESTIMATING TIDALLY DRIVEN MIXING. *Geophysical Research Letters*, *29*(23), 21-1-21–24. https://doi.org/10.1029/2002GL015633

Stigebrandt, A. (1976). Vertical diffusion driven by internal waves in a sill fjord. *Journal of Physical Oceanography*, *6*(4), 486–495.

Stigebrandt, A. (1987). A Model for the Vertial Circulation of the Baltic Deep Water. *Journal of Physical Oceanography*, *17*(10), 1772–1785. https://doi.org/10.1175/1520-0485(1987)017<1772:AMFTVC>2.0.CO;2

van der Lee, E. M., & Umlauf, L. (2011). Internal wave mixing in the Baltic Sea: Near-inertial waves in the absence of tides. *Journal of Geophysical Research*, *116*(C10), C10016. https://doi.org/10.1029/2011JC007072

Waterhouse, A. F., MacKinnon, J. A., Nash, J. D., Alford, M. H., Kunze, E., Simmons, H. L., Polzin, K. L., Laurent, L. C. S., Sun, O. M., Pinkel, R., Talley, L. D., Whalen, C. B., Huussen, T. N., Carter, G. S., Fer, I., Waterman, S., Garabato, A. C. N., Sanford, T. B., & Lee, C. M. (2014). Global Patterns of Diapycnal Mixing from Measurements of the Turbulent Dissipation Rate. *Journal of Physical Oceanography*, *44*(7), 1854–1872. https://doi.org/10.1175/JPO-D-13-0104.1

Welch, W. T., Smolarkiewicz, P., Rotunno, R., & Boville, B. A. (2001). The large-scale effects of flow over periodic mesoscale topography. *Journal of the Atmospheric Sciences*, *58*(12), 1477–1492.

Wüest, A., & Lorke, A. (2003). Small-Scale Hydrodynamics in Lakes. *Annual Review of Fluid Mechanics*, *35*(1), 373–412. https://doi.org/10.1146/annurev.fluid.35.101101.161220